

Quench-Probe Setup as an Analyzer of Fractionalized Entanglement Spreading

Nicolas P. Bauer,^{1,2,*} Jan Carl Budich,^{3,2} Björn Trauzettel,^{1,2} and Alessio Calzona^{1,2}

¹*Institute of Theoretical Physics and Astrophysics, University of Würzburg, Germany*

²*Würzburg-Dresden Cluster of Excellence ct.qmat, Germany*

³*Institute of Theoretical Physics, Technische Universität Dresden, Germany*

(Dated: July 12, 2022)

We propose a novel spatially inhomogeneous setup for revealing quench-induced fractionalized excitations in entanglement dynamics. In this quench-probe setting, the region undergoing a quantum quench is tunnel-coupled to a static region, the probe. Subsequently, the time-dependent entanglement signatures of a tunable subset of excitations propagating to the probe are monitored. We exemplify the power of this generic approach by identifying a unique dynamical signature associated with the presence of an isolated Majorana zero mode in the post-quench Hamiltonian. In this case excitations emitted from the topological part of the system give rise to a fractionalized jump of $\log(2)/2$ in the entanglement entropy of the probe. This dynamical effect is highly sensitive to the localized nature of the Majorana zero mode, but does not require the preparation of a topological initial state.

Introduction.— Identifying physical signatures to distinguish and understand phases of matter occurring in nature is a main objective of research in physics. There, dynamical approaches probing a system far from thermal equilibrium have become increasingly important. In particular, quantum quenches, i.e. abrupt changes of parameters in the Hamiltonian, have enabled unprecedented insights into structure and dynamics of quantum matter, both in theory [1–3] and experiment [4–8]. A prominent example is provided by the prediction and observation of non-equilibrium topological invariants [9–23] that probe topological properties of matter without requiring the preparation of a topological equilibrium state.

As a powerful and genuinely quantum-mechanical diagnostic tool, the time-evolution of entanglement has been widely investigated [1, 3, 24, 25], including dynamical signatures of topology such as protected crossings in the entanglement spectrum [26–30]. In homogeneous integrable systems, the spreading of entanglement after a quench is closely related to the propagation of pairs of entangled quasiparticle excitations with opposite momenta [25, 31–33]. For more complex scenarios, involving for example periodic spatial modulations [34] or open systems [35, 36], richer entanglement structures related to quench-induced excitations represent a broad frontier of ongoing research [37–44].

In this Letter, we propose a novel approach for the study of entanglement dynamics in complex systems to selectively analyze a subset of quench-induced excitations. This enables us to identify unique features in the spreading of entanglement, such as fractional jumps of the entanglement entropy (EE), and to directly relate their presence to the existence of non-trivial eigenmodes in the post-quench Hamiltonian, e.g. topological localized modes. This remarkable capability stems from the hybrid nature of our proposed setup, sketched in Fig. 1(a), where only a part of the system (Q) is quenched while the entanglement is measured in a different (static)

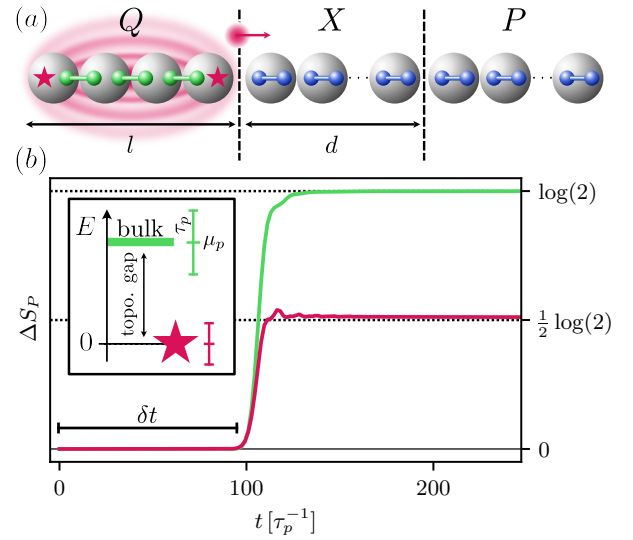


FIG. 1. (a) Hybrid quench-probe setup. A 1D Kitaev chain Q , which undergoes a quantum quench across its topological phase transition, is tunnel-coupled at its right end to the trivial regions X and P . Quench-induced excitations are selectively transmitted through X and eventually reach P , whose time-dependent entanglement properties are monitored. (b) Quantized jumps in the entanglement entropy (EE) of the probe. When the latter is selectively coupled to the right MZM (red star), a robust fractional increase of the EE $\Delta S_P = \log(2)/2$ is observed (red line), which is half of the increase observed when the probe is coupled to the fermionic bulk flatband of the Kitaev chain (green line). A schematic of the energy-selective coupling, allowed by the quench probe approach, is provided in the inset. Our choice of parameters is given in the caption of Fig. 2, apart from $\tau^f = \Delta^f = 11.76 \tau_p$.

region (P), the two being coupled via a (static) separation layer (X). This quench-probe approach provides a new perspective for the analysis of entanglement spreading in highly inhomogeneous systems, paving the way for novel observations that complement the study of (almost) homogeneous setups [13, 14, 31, 32, 34, 44–47].

As a specific case study, we use our approach to analyze the dynamics of the entanglement generated by a localized Majorana zero mode (MZM), hosted by a Kitaev chain (KC) [48–50]. This led us to the discovery of quantized jumps in the EE of the probe with fractional amplitude

$$\Delta S_P = \frac{\log(2)}{2}. \quad (1)$$

An example is provided by the red line in Fig. 1(b). Such a fractional increase, which is associated with the fractional entropy of a single MZM [51–53], clearly differs from the conventional EE increase $\Delta S_P = \log(2)$ that originates from an ordinary fermionic flat band [see the green line in Fig. 1(b)]. The quantization is robust with respect to parameter variations but highly sensitive to the hybridization of the MZM with other modes. These findings, representing a novel dynamical signature associated with a truly isolated MZM, are corroborated by the additional analysis of the mutual information (MI) shared between Q and P [30, 36, 46], which allows us to identify spurious contributions to the EE and highlight the fractional entanglement jumps. Importantly, the observation of this topological signature only requires the post-quench Hamiltonian to be topological, while the system can be prepared in a trivial thermal state.

Hybrid quench-probe setup.— We consider the system depicted in Fig. 1(a), consisting of the three parts labeled Q , X , and P . The first one, Q , is the one eventually undergoing a quantum quench and it is an l -site KC described by the Hamiltonian

$$H^Q = \mu \sum_{i=1}^l c_i^\dagger c_i + \sum_{i=1}^{l-1} \left(\frac{\tau}{2} c_i^\dagger c_{i+1} + \frac{\Delta}{2} c_i c_{i+1} + \text{h.c.} \right). \quad (2)$$

The operators c_i^\dagger (c_i) create (annihilate) a spinless fermion at site i , μ is the chemical potential, τ the nearest-neighbor hopping amplitude and Δ the superconducting pairing amplitude. For simplicity, we consider those parameters to be non-negative real numbers. The KC features two different gapped phases, a trivial one for $|\mu| > \tau$ and a topological one for finite Δ and $|\mu| < \tau$. At the topological sweet spot (TSS), i.e. $\tau = \Delta$ and $\mu = 0$, the analysis of H^Q in terms of Majorana operators $c_j = \frac{1}{2}(i\gamma_{2i-1} + \gamma_{2i})$ reveals the presence of two completely isolated MZMs at the two open ends of the chain $[\gamma_1, H^Q] = [\gamma_{2l}, H^Q] = 0$. See the red stars in Fig. 1(a). The bulk of the KC at the TSS is described by a flat band at finite energy $E^Q = \tau$. Deviations from the TSS (within the topological phase) imply an exponential leakage of the MZMs into the bulk, whose spectrum acquires then a finite bandwidth $E^Q(k) = \sqrt{(\tau \cos(k) + \mu)^2 + (\Delta \sin(k))^2}$ [50].

The remaining $N - l$ sites of the system are described

by a tight-binding Hamiltonian

$$H^{XP} = \sum_{i=l+1}^N \mu_p c_i^\dagger c_i + \frac{1}{2} \sum_{j=l+1}^{N-1} \tau_p (c_j^\dagger c_{j+1} + \text{h.c.}), \quad (3)$$

with chemical potential μ_p and hopping amplitude τ_p . The corresponding spectrum reads

$$E^{XP}(k) = \mu_p + \tau_p \cos(k). \quad (4)$$

The first d sites, i.e. the ones between $l < j \leq l+d$, form the separation layer X , while the probe region P consists of the remaining sites with $l+d < j \leq N$. The presence of a finite X allows us to consider regimes in which the probe region P is exclusively affected by quench-induced excitations that propagate ballistically in the chain, filtering out possible contributions to the entanglement associated with the Q - X interface. Regions Q and X are connected via a standard tunneling Hamiltonian

$$H^T = \frac{\tau_p}{2} (c_l^\dagger c_{l+1} + \text{h.c.}) = \frac{\tau_p}{4} [(i\gamma_{2l-1} + \gamma_{2l})c_{l+1} + \text{h.c.}]. \quad (5)$$

It is particularly instructive to express fermions in terms of the corresponding Majorana operators. At the TSS, γ_{2l} is an isolated MZM while γ_{2l-1} , together with γ_{2l-2} , belongs to an ordinary fermionic mode of the flat bulk band of the KC. Coupled Majorana operators belonging to the bulk of the KC are depicted by green circles in Fig. 1(a). By properly tuning the parameters of the system, it is thus possible to define two separated regimes. For $|\mu_p| < \tau_p \ll \tau$ the probe is exclusively coupled to the MZM at the right end of the topological KC. By contrast, for $|\mu_p| \sim \tau \gg \tau_p$, the probe is coupled to the bulk band [54]. A sketch of this energy-selective coupling is provided in the inset of Fig. 1(b). The exploitation of energy and spatial sensitivity, together with the presence of a separation layer X , differentiates our proposal from other quench-probe scenarios, such as the ones discussed in [55–57].

Quench procedure.— The quench of region Q consists in the abrupt change, at $t = 0$, of the parameters $(\mu^i, \tau^i, \Delta^i) \rightarrow (\mu^f, \tau^f, \Delta^f)$. We assume the system to be initially prepared in the ground state $|\psi_0\rangle$ of the initial Hamiltonian $H^i = H^Q(\mu^i, \tau^i, \Delta^i) + H^{XP} + H^T$. For $t \geq 0$, the time evolution of the system is instead controlled by the final Hamiltonian $H^f = H^Q(\mu^f, \tau^f, \Delta^f) + H^{XP} + H^T$. With respect to H^f , the state $|\psi_0\rangle$ consists of several quasiparticle excitations, that are emitted in both directions from every site in the quenched region Q . Following Refs. [31–33], those counter-propagating quasiparticles are entangled between each other and their motion, bounded by the Lieb-Robinson limit [58], is responsible for spreading of correlations and entanglement within the system. For a wide range of homogeneous systems, these quasiparticles are produced in uncorrelated

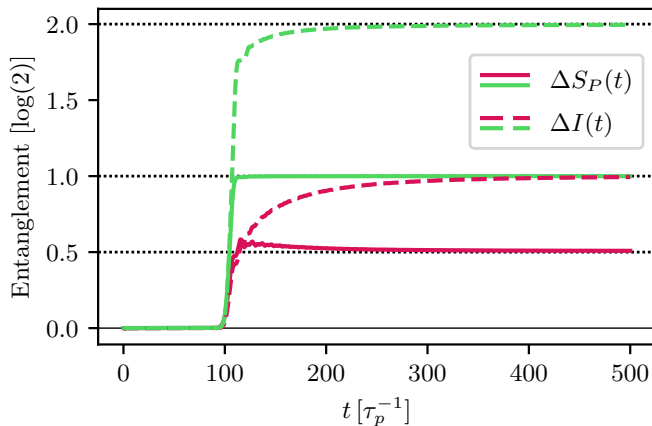


FIG. 2. Quantized jumps in the EE $\Delta S_P(t)$ (solid lines) and MI $\Delta I(t)$ (dashed lines), in units of $\log_2(2)$ for a probe coupled either to the MZM (red lines) or the fermionic bulk modes (green lines). Our parameter choice is $(\mu^i, \tau^i = \Delta^i = \tau_p) \rightarrow (\mu^f = 0, \tau^f = \Delta^f = 20\tau_p)$; $N = 500, l = 4, d = 100, t_0 = 10$ and we couple to the MZM (fermionic bulk modes) using $\mu_p = 0$ ($\mu_p = \tau_f$).

pairs, each one consisting of two entangled quasiparticles with opposite momenta [59–63]. The physics is richer in presence of interactions and/or inhomogeneities, which can lead to the presence of quasiparticle multiplets and non-trivial correlations [34, 42–44]. When H_f is chosen in the topological regime, our system is spatially inhomogeneous due to the presence of a pair of isolated MZMs. This observation naturally raises the question whether the quasiparticles originating from the MZMs differ from the ones associated with the fermionic bulk of the KC. Our proposed quench-probe setup proves to be particularly effective in providing an affirmative answer to this question.

Entanglement dynamics.— The simplest way to analyze the entanglement properties of P is to compute its EE, defined as

$$S_P(t) = -\text{Tr}[\rho_P(t) \log(\rho_P(t))]. \quad (6)$$

Here, $\rho_P(t)$ is the reduced density matrix of the probe $\rho_P(t) = \text{Tr}_{QX}[\rho(t)]$, whose spectrum can be calculated from the single-particle correlation matrix [64–66]. The time-dependent variation of the EE after a quench to the TSS is shown in Fig. 1(b), where we plot $\Delta S_P(t) = S_P(t) - S_P(0)$ considering a selective coupling either to the isolated MZM (red line) or to the flat fermionic bulk band (green line). After a finite time delay δt , we observe jumps in the EE that eventually reach either the trivial quantized value $\log(2)$ (for the coupling to the bulk) or an anomalous fractional value $\log(2)/2$ (for the coupling to the MZM). Consistently with the quasiparticle picture, the time delay satisfies $\delta t \sim d\tau_p^{-1}$. It can be interpreted as the time-of-flight associated with the excitations, emitted from the last site of Q , that travels

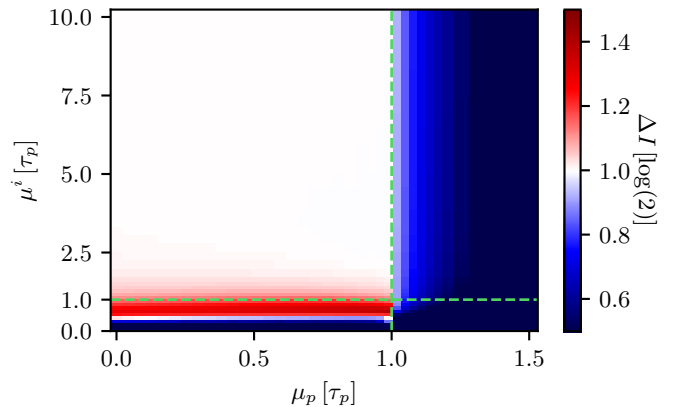


FIG. 3. Quantization of the MI increase. ΔI is plotted as a function of μ^i and μ_p (units τ_p). The dashed horizontal (vertical) line indicates the topological phase transition of the initial Hamiltonian (the transition between a gapless and gapped probe). Our choice of parameters is given in the caption of Fig. 2 apart from $N = 2000, t_\infty = 3000, t_0 = 80$.

thorough the d sites of X at the maximum group velocity τ_p [see Eq. (4)]. The lack of a steady linear increase of $\Delta S_P(t)$, typically observed in homogeneous systems [31–33], can be understood in terms of the vanishing group velocity in the bulk of the KC at the TSS. This effectively freezes all the quasiparticles emitted in Q with the only exception of the ones related to γ_{2l-1} and γ_{2l} , which are directly connected to X via H^T . Those quasiparticles are ultimately responsible for the quantized jumps discussed before. Analogous features can be observed in Fig. 2 (solid lines), where the same analysis is performed for different values of $\Delta^f = \tau^f$.

To strengthen the connection between the anomalous fractional jump of the EE and the presence of an isolated MZM, we additionally compute the time-dependent mutual information (MI) shared between the probe P and the quenched region Q . It is defined as

$$I(t) = S_Q(t) + S_P(t) - S_{Q \cup P}(t) \quad (7)$$

and quantifies the total amount of correlations between the two disjoint regions [30, 36, 46], eliminating spurious contributions to S_P coming from the separation layer X and not from the quenched region Q . The increase of MI $\Delta I(t) = I(t) - I(t_0)$, where $t_0 \lesssim \delta t$ and $I(t_0) \rightarrow 0$ for large d [54], is plotted in Fig. 2 (dashed lines). It shares its main features with ΔS_P . In particular, when the probe is effectively coupled to the fermionic bulk of the KC (dashed lines), ΔI saturates at $2\log(2)$, indicating that P and Q share a conventional fermionic mode [54]. By contrast, when the probe is coupled to the isolated MZM (solid lines), the height of the increase is halved and ΔI saturates at $\log(2)$. In the following, we carefully analyze the MZM case.

Anomalous quantization.— After a sufficiently long time t_∞ and in the large d limit [67], $\Delta I(t_\infty)$ shows

a high degree of quantization and robustness. Indeed, as long as the probe is gapless and the initial Hamiltonian features a large trivial gap (thus ensuring regions Q and X to be initially decoupled), the MI saturates at $\Delta I(t_\infty) = \log(2)$ without the need of fine-tuning, as shown by the large white area in Fig. 3. This anomalous quantization is robust against finite temperature effects and deviations of H^f from the TSS [54]. The latter leads to two main effects, (i) a finite band-width of the fermionic bulk band and (ii) an exponentially suppressed leakage of the MZMs towards the bulk of the KC. Both effects have no consequences on the long-time entanglement properties of the probe, provided that the KC is long enough to avoid MZM hybridization and that the energy-selective coupling is effective in completely decoupling the probe from the bulk band. As for the robustness at finite temperature, we show that the quantization of the MI is retained even when the system is initialized in a thermal trivial state of H^i at finite temperature T , as long as the latter remains smaller than the topological gap $T \ll \tau^f = \Delta^f$ [54].

In contrast to the above-mentioned robustness against temperature, $\Delta I(t_\infty)$ display a remarkable sensitivity to the presence of spurious MZM hybridizations. Hence the isolated nature of the right MZM is the origin of the anomalous quantization. To further substantiate this point, we consider an additional contribution to the Hamiltonian $H_{\gamma\gamma} = i\tau_{\gamma\gamma}\gamma_1\gamma_{2l} + \text{h.c.}$, which directly couples the Majorana operators γ_1 and γ_{2l} at the two ends of the KC. A finite amplitude $\tau_{\gamma\gamma} > 0$ leads to a hybridization of the two MZMs, which then acquire a finite energy. Remarkably, even a small hybridization $0 < \tau_{\gamma\gamma} \ll \tau_p$ determines noticeable deviations from the quantized values of MI that emerge on a time scale given by $\tau_{\gamma\gamma}^{-1}$ [54]. The high sensitivity to the isolated nature of the MZM represents a powerful tool to clearly distinguish topological MZMs from accidental trivial modes close to zero energy.

Transient dynamics.— Our quench-probe setup features a useful knob, i.e. the size d of the X region, which can significantly enrich the analysis of the post-quench transient entanglement dynamics. Indeed, a careful study of $I(t)$ as a function of d (plotted in Fig. 4) reveals the coexistence of a fixed and a propagating component of the correlations contributing to the MI. Let us explain this point by carefully inspecting Fig. 4, from right to left. If the probe region is too far away from Q , the quench-induced excitations have not yet reached P and the MI is basically zero. This explains the large triangular gray area in Fig. 4, which is bounded by the Lieb-Robinson limit $d = t\tau_p$ (black dashed line) [68]. To the left of the Lieb-Robinson line, the MI increases as the probe includes an increasing number of sites entangled with Q (orange region). The MI reaches $I \simeq 0.95 \log(2)$ close to the red-dotted line, which we attribute to the propagation of excitations of finite but smaller group velocity than τ_p . To the left of the red-dotted line, the

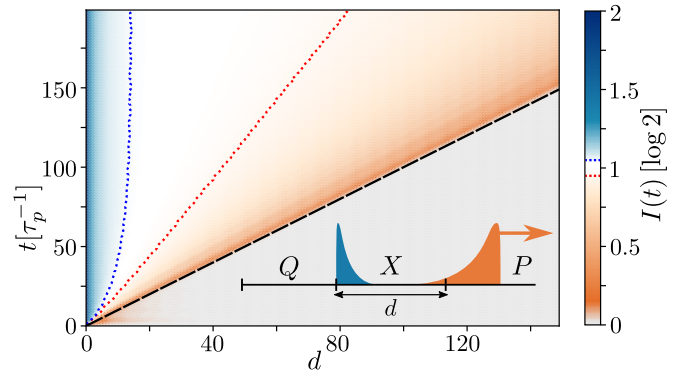


FIG. 4. MI as a function of d and time t . The red(blue)-dotted line corresponds to $I/\log 2 = 0.95$ (1.05). The black-dashed line shows the Lieb-Robinson limit $d = t\tau_p$. The inset shows a sketch of the fixed (blue) and propagating (orange) contributions to the MI. We choose the parameters given in the caption of Fig. 2 apart from $N = 350, l = 10$.

MI features a plateau around the anomalous quantized value of $\log(2)$ (white region), the regime described in the previous paragraphs. For small d , i.e. when the probe region starts to include sites close to the Q - X interface, the MI increases again and displays values above $\log(2)$ (blue region). Interestingly, the correlations responsible for this additional increase of MI do not propagate within the probe, as shown by the blue-dotted line, corresponding to $I \simeq 1.05 \log(2)$, which is asymptotically vertical. Finally, for $d = 0$, the MI reaches the conventional quantized value of $I = 2 \log(2)$. At a given (large) time, we can thus identify two groups of sites that are entangled with Q , a propagating one and a fixed one (pinned at the Q - X interface), as sketched in the inset of Fig. 4. The precise and robust quantization of ΔI , shown in Fig. 3, can be therefore understood as the result of a dynamical phenomenon, namely the separation of the correlations between Q and P into two different components.

Discussion and conclusions.— Our quench-probe setup allows us to identify a robust dynamical effect associated with the presence of an isolated MZM, hosted by the post-quench topological Hamiltonian. The observation of this effect, consisting of particular fractional quantized jumps in the entanglement properties of the probe, only requires the preparation of the system in a trivial state. It is therefore within experimental reach.

These results clearly show the potential and the flexibility of our quench-probe approach. Moreover, by using the separation region X as an additional knob, we envision more detailed studies of the ballistic propagation of quench-generated quasiparticles in dispersive mediums, isolating and characterizing the entanglement contribution associated with each individual mode. Finally, the study of systems featuring multiple quenched regions Q_i , connected to a single probe P via a network of separation layers

could lead to the emergence of non-local and interference effects affecting the dynamics of entanglement spreading.

This work was supported by the Würzburg-Dresden Cluster of Excellence ct.qmat, EXC2147, project-id 390858490, and the DFG (SPP 1666 and SFB 1170). We thank the Bavarian Ministry of Economic Affairs, Regional Development and Energy for financial support within the High-Tech Agenda Project “Bausteine für das Quanten Computing auf Basis topologischer Materialien”.

* Email: nicolas.bauer@physik.uni-wuerzburg.de

- [1] C. Gogolin and J. Eisert, Equilibration, thermalisation, and the emergence of statistical mechanics in closed quantum systems, *Reports on Progress in Physics* **79**, 056001 (2016).
- [2] A. Polkovnikov, K. Sengupta, A. Silva, and M. Vengalattore, Colloquium: Nonequilibrium dynamics of closed interacting quantum systems, *Rev. Mod. Phys.* **83**, 863 (2011).
- [3] F. H. L. Essler and M. Fagotti, Quench dynamics and relaxation in isolated integrable quantum spin chains, *Journal of Statistical Mechanics: Theory and Experiment* **2016**, 064002 (2016).
- [4] T. Kinoshita, T. Wenger, and D. S. Weiss, A quantum newton’s cradle, *Nature* **440**, 900 (2006).
- [5] M. Gring, M. Kuhnert, T. Langen, T. Kitagawa, B. Rauer, M. Schreitl, I. Mazets, D. A. Smith, E. Demler, and J. Schmiedmayer, Relaxation and prethermalization in an isolated quantum system, *Science* **337**, 1318 (2012).
- [6] M. Cheneau, P. Barmettler, D. Poletti, M. Endres, P. Schauß, T. Fukuhara, C. Gross, I. Bloch, C. Kollath, and S. Kuhr, Light-cone-like spreading of correlations in a quantum many-body system, *Nature* **481**, 484 (2012).
- [7] T. Langen, R. Geiger, M. Kuhnert, B. Rauer, and J. Schmiedmayer, Local emergence of thermal correlations in an isolated quantum many-body system, *Nature Physics* **9**, 640 (2013).
- [8] I. Bloch, J. Dalibard, and W. Zwerger, Many-body physics with ultracold gases, *Rev. Mod. Phys.* **80**, 885 (2008).
- [9] P. Hauke, M. Lewenstein, and A. Eckardt, Tomography of band insulators from quench dynamics, *Phys. Rev. Lett.* **113**, 045303 (2014).
- [10] S. Vajna and B. Dóra, Topological classification of dynamical phase transitions, *Phys. Rev. B* **91**, 155127 (2015).
- [11] J. C. Budich and M. Heyl, Dynamical topological order parameters far from equilibrium, *Phys. Rev. B* **93**, 085416 (2016).
- [12] N. Goldman, J. C. Budich, and P. Zoller, Topological quantum matter with ultracold gases in optical lattices, *Nature Physics* **12**, 639 (2016).
- [13] A. Eckardt, Colloquium: Atomic quantum gases in periodically driven optical lattices, *Rev. Mod. Phys.* **89**, 011004 (2017).
- [14] N. R. Cooper, J. Dalibard, and I. B. Spielman, Topological bands for ultracold atoms, *Rev. Mod. Phys.* **91**, 015005 (2019).
- [15] A. Bermudez, D. Patanè, L. Amico, and M. A. Martin-Delgado, Topology-induced anomalous defect production by crossing a quantum critical point, *Phys. Rev. Lett.* **102**, 135702 (2009).
- [16] M. D. Caio, N. R. Cooper, and M. J. Bhaseen, Quantum quenches in chern insulators, *Phys. Rev. Lett.* **115**, 236403 (2015).
- [17] Y. Hu, P. Zoller, and J. C. Budich, Dynamical buildup of a quantized hall response from nontopological states, *Phys. Rev. Lett.* **117**, 126803 (2016).
- [18] C. Wang, P. Zhang, X. Chen, J. Yu, and H. Zhai, Scheme to measure the topological number of a chern insulator from quench dynamics, *Phys. Rev. Lett.* **118**, 185701 (2017).
- [19] W. Sun, C.-R. Yi, B.-Z. Wang, W.-W. Zhang, B. C. Sanders, X.-T. Xu, Z.-Y. Wang, J. Schmiedmayer, Y. Deng, X.-J. Liu, S. Chen, and J.-W. Pan, Uncover topology by quantum quench dynamics, *Phys. Rev. Lett.* **121**, 250403 (2018).
- [20] H. Hu and E. Zhao, Topological invariants for quantum quench dynamics from unitary evolution, *Phys. Rev. Lett.* **124**, 160402 (2020).
- [21] M. McGinley and N. R. Cooper, Topology of one-dimensional quantum systems out of equilibrium, *Physical review letters* **121**, 090401 (2018).
- [22] N. Fläschner, D. Vogel, M. Tarnowski, B. S. Rem, D.-S. Lühmann, M. Heyl, J. C. Budich, L. Mathey, K. Sengstock, and C. Weitenberg, Observation of dynamical vortices after quenches in a system with topology, *Nature Physics* **14**, 265 (2017).
- [23] J. A. Marks, M. Schüler, and T. P. Devereaux, Dynamical signatures of symmetry protected topology following symmetry breaking, *Phys. Rev. Research* **3**, 023137 (2021).
- [24] P. Calabrese, F. H. L. Essler, and G. Mussardo, Introduction to ‘quantum integrability in out of equilibrium systems’, *Journal of Statistical Mechanics: Theory and Experiment* **2016**, 064001 (2016).
- [25] P. Calabrese, Entanglement spreading in non-equilibrium integrable systems, *SciPost Phys. Lect. Notes*, 20 (2020).
- [26] Z. Gong and M. Ueda, Topological entanglement-spectrum crossing in quench dynamics, *Phys. Rev. Lett.* **121**, 250601 (2018).
- [27] L. Pastori, S. Barbarino, and J. C. Budich, Signatures of topology in quantum quench dynamics and their interrelation, *Phys. Rev. Research* **2**, 033259 (2020).
- [28] S. Sayyad, J. Yu, A. G. Grushin, and L. M. Sieberer, Entanglement spectrum crossings reveal non-hermitian dynamical topology, *Phys. Rev. Research* **3**, 033022 (2021).
- [29] T. Micallo, V. Vitale, M. Dalmonte, and P. Fromholz, Topological entanglement properties of disconnected partitions in the Su-Schrieffer-Heeger model, *SciPost Phys. Core* **3**, 12 (2020).
- [30] S. Mondal, S. Bandyopadhyay, S. Bhattacharjee, and A. Dutta, Detecting topological phase transitions through entanglement between disconnected partitions in a kitaev chain with long-range interactions, *Phys. Rev. B* **105**, 085106 (2022).
- [31] P. Calabrese and J. Cardy, Evolution of entanglement entropy in one-dimensional systems, *Journal of Statistical Mechanics: Theory and Experiment* **2005**, P04010 (2005).
- [32] P. Calabrese and J. Cardy, Quantum quenches in 1+1 dimensional conformal field theories, *Journal of Statis-*

- tical Mechanics: Theory and Experiment **2016**, 064003 (2016).
- [33] H. Kim and D. A. Huse, Ballistic spreading of entanglement in a diffusive nonintegrable system, *Phys. Rev. Lett.* **111**, 127205 (2013).
 - [34] A. Bastianello and P. Calabrese, Spreading of entanglement and correlations after a quench with intertwined quasiparticles, *SciPost Phys.* **5**, 33 (2018).
 - [35] V. Alba and F. Carollo, Spreading of correlations in markovian open quantum systems, *Phys. Rev. B* **103**, L020302 (2021).
 - [36] S. Maity, S. Bandyopadhyay, S. Bhattacharjee, and A. Dutta, Growth of mutual information in a quenched one-dimensional open quantum many-body system, *Phys. Rev. B* **101**, 180301 (2020).
 - [37] V. Alba and F. Heidrich-Meisner, Entanglement spreading after a geometric quench in quantum spin chains, *Phys. Rev. B* **90**, 075144 (2014).
 - [38] V. Alba, Entanglement and quantum transport in integrable systems, *Phys. Rev. B* **97**, 245135 (2018).
 - [39] B. Bertini, M. Fagotti, L. Piroli, and P. Calabrese, Entanglement evolution and generalised hydrodynamics: non-interacting systems, *Journal of Physics A: Mathematical and Theoretical* **51**, 39LT01 (2018).
 - [40] V. Alba, B. Bertini, and M. Fagotti, Entanglement evolution and generalised hydrodynamics: interacting integrable systems, *SciPost Phys.* **7**, 5 (2019).
 - [41] V. Alba, Towards a generalized hydrodynamics description of rényi entropies in integrable systems, *Phys. Rev. B* **99**, 045150 (2019).
 - [42] B. Bertini, E. Tartaglia, and P. Calabrese, Quantum quench in the infinitely repulsive hubbard model: the stationary state, *Journal of Statistical Mechanics: Theory and Experiment* **2017**, 103107 (2017).
 - [43] B. Bertini, E. Tartaglia, and P. Calabrese, Entanglement and diagonal entropies after a quench with no pair structure, *Journal of Statistical Mechanics: Theory and Experiment* **2018**, 063104 (2018).
 - [44] A. Bastianello and M. Collura, Entanglement spreading and quasiparticle picture beyond the pair structure, *SciPost Phys.* **8**, 45 (2020).
 - [45] V. Alba and P. Calabrese, Entanglement and thermodynamics after a quantum quench in integrable systems, *Proceedings of the National Academy of Sciences* **114**, 7947 (2017).
 - [46] V. Alba and P. Calabrese, Entanglement dynamics after quantum quenches in generic integrable systems, *SciPost Physics* **4**, 10.21468/scipostphys.4.3.017 (2018).
 - [47] G. D. Giulio, R. Arias, and E. Tonni, Entanglement hamiltonians in 1d free lattice models after a global quantum quench, *Journal of Statistical Mechanics: Theory and Experiment* **2019**, 123103 (2019).
 - [48] E. Majorana, Teoria simmetrica dell'elettrone e del positrone, *Il Nuovo Cimento* **14**, 171 (1937).
 - [49] A. Y. Kitaev, Unpaired majorana fermions in quantum wires, *Physics-Uspekhi* **44**, 131 (2001).
 - [50] J. Alicea, New directions in the pursuit of majorana fermions in solid state systems, *Reports on Progress in Physics* **75**, 076501 (2012).
 - [51] E. Sela, Y. Oreg, S. Plugge, N. Hartman, S. Lüscher, and J. Folk, Detecting the universal fractional entropy of majorana zero modes, *Phys. Rev. Lett.* **123**, 147702 (2019).
 - [52] S. Smirnov, Majorana tunneling entropy, *Phys. Rev. B* **92**, 195312 (2015).
 - [53] J. F. Silva, L. G. G. V. D. da Silva, and E. Vernek, Robustness of the kondo effect in a quantum dot coupled to majorana zero modes, *Phys. Rev. B* **101**, 075428 (2020).
 - [54] See the supplemental material. URL_will_be_inserted_by_publisher.
 - [55] A. Calzona, F. M. Gambetta, F. Cavaliere, M. Carrega, and M. Sassetti, Quench-induced entanglement and relaxation dynamics in luttinger liquids, *Physical Review B* **96**, 10.1103/physrevb.96.085423 (2017).
 - [56] A. Calzona, F. M. Gambetta, M. Carrega, F. Cavaliere, T. Schmidt, and M. Sassetti, Universal scaling of quench-induced correlations in a one-dimensional channel at finite temperature, *SciPost Physics* **4**, 10.21468/scipostphys.4.5.023 (2018).
 - [57] P. Ruggiero, P. Calabrese, L. Foini, and T. Giamarchi, Quenches in initially coupled tomonaga-luttinger liquids: a conformal field theory approach, *SciPost Physics* **11**, 10.21468/scipostphys.11.3.055 (2021).
 - [58] E. H. Lieb and D. W. Robinson, The finite group velocity of quantum spin systems, *Communications in Mathematical Physics* **28**, 251 (1972).
 - [59] M. A. Cazalilla, A. Iucci, and M.-C. Chung, Thermalization and quantum correlations in exactly solvable models, *Phys. Rev. E* **85**, 011133 (2012).
 - [60] D. Schuricht and F. H. L. Essler, Dynamics in the ising field theory after a quantum quench, *Journal of Statistical Mechanics: Theory and Experiment* **2012**, P04017 (2012).
 - [61] M. A. Cazalilla, Effect of suddenly turning on interactions in the luttinger model, *Phys. Rev. Lett.* **97**, 156403 (2006).
 - [62] J. De Nardis, B. Wouters, M. Brockmann, and J.-S. Caux, Solution for an interaction quench in the lieb-liniger bose gas, *Phys. Rev. A* **89**, 033601 (2014).
 - [63] M. Brockmann, J. D. Nardis, B. Wouters, and J.-S. Caux, Néel-XXZ state overlaps: odd particle numbers and lieb-liniger scaling limit, *Journal of Physics A: Mathematical and Theoretical* **47**, 345003 (2014).
 - [64] I. Peschel, Calculation of reduced density matrices from correlation functions, **36**, L205.
 - [65] I. Peschel and V. Eisler, Reduced density matrices and entanglement entropy in free lattice models, *Journal of Physics A: Mathematical and Theoretical* **42**, 504003 (2009).
 - [66] G. Vidal, J. I. Latorre, E. Rico, and A. Kitaev, Entanglement in quantum critical phenomena, *Phys. Rev. Lett.* **90**, 227902 (2003).
 - [67] Note that the maximum time that can be actually studied is limited by the finite number of sites N and the consequent reflections of quasiparticle at the right end of the system. Ad for the full d dependence, it is discussed later, in Fig. 4.
 - [68] The small deviations from $I = 0$ which can be observed below the dashed line for small d are a consequence of the non-local nature of the MI and they are not present in the EE [54].
 - [69] C. Holzhey, F. Larsen, and F. Wilczek, Geometric and renormalized entropy in conformal field theory, *Nuclear Physics B* **424**, 443 (1994).
 - [70] L. Levy and M. Goldstein, Entanglement and disordered-enhanced topological phase in the kitaev chain, *Universe* **5**, 33 (2019).
 - [71] P. Calabrese and J. Cardy, Entanglement entropy and

quantum field theory, Journal of Statistical Mechanics:
Theory and Experiment **2004**, P06002 (2004).

APPENDIX

In the main text, we proposed a novel quench-probe setup for the study of entanglement dynamics and demonstrated its capabilities by showing a novel fractional entanglement signature induced by a single Majorana zero mode. The main goal of this supplemental material is to provide additional technical details about the origin and robustness of this signature. This includes a discussion about origin of the fractional entanglement signature in the mutual information in (Section A), an analysis of the initial entanglement (Section B), a study of the dispersion of the entanglement quasiparticles in the X region (Section C), and an extended survey about the robustness of the fractional entanglement signature (Section D).

Appendix A: Majornana-related MI

The goal of this section is to compute the entanglement entropy (EE) and the mutual information (MI) for subsystems that share either an ordinary fermion or a single Majorana. To this end, we consider a toy model consisting of three physical fermionic sites whose creation (annihilation) operators read c_j (c_j^\dagger) with $j = 1, 2, 3$. In the following, we use the eigenvalues of the number operators $n_j = c_j^\dagger c_j$ to label the states as $|n_1 n_2 n_3\rangle$. As discussed in the main text, it is convenient to describe the system in terms of Majorana operators γ_j that satisfy

$$\begin{cases} c_j = \frac{1}{2}(i\gamma_{2j-1} + \gamma_{2j}) \\ c_j^\dagger = \frac{1}{2}(-i\gamma_{2j-1} + \gamma_{2j}) \end{cases} \Leftrightarrow \begin{cases} \gamma_{2j} = c_j + c_j^\dagger \\ \gamma_{2j-1} = i(c_j^\dagger - c_j) \end{cases}. \quad (\text{A.1})$$

We start our analysis by considering a simple pure state of the system,

$$|\psi_F\rangle = \frac{|100\rangle + |010\rangle}{\sqrt{2}}, \quad (\text{A.2})$$

which is an eigenstate $F|\psi_F\rangle = |\psi_F\rangle$ of the Hermitian operator $F = c_1^\dagger c_2 + c_2^\dagger c_1$. As the latter describes the tunneling of one fermion between the first two sites, $|\psi_F\rangle$ features a delocalized fermion distributed over the first two sites. It forms a Bell state. A straightforward analysis of the entanglement entropies associated to every single site leads to $S_1^F = S_2^F = \log(2)$ and $S_3^F = S_{1\cup 2}^F = 0$. The MI between the first and the second site is thus given by

$$I^F = S_1^F + S_2^F - S_{1\cup 2}^F = 2\log(2). \quad (\text{A.3})$$

The expression of the operator $F = (i\gamma_2\gamma_3 - i\gamma_1\gamma_4)/2$ in terms of Majorana operators shows that a fermionic tunneling actually corresponds to two Majorana tunneling terms, expressed via the parity operators $P_{ij} = i\gamma_i\gamma_j$ (remember that $\gamma_i^\dagger = \gamma_i$). This raises the question about the entanglement properties of the system when it is in an eigenstate of only a *single* Majorana tunneling term, say P_{23} . To this end, we consider the state

$$|\psi_M\rangle = \frac{|100\rangle + |010\rangle + |001\rangle + |111\rangle}{2} \quad (\text{A.4})$$

that indeed satisfies

$$\begin{aligned} P_{23}|\psi_M\rangle &= (F + c_1c_2 + c_2^\dagger c_1^\dagger)|\psi_M\rangle \\ &= \frac{|010\rangle + |100\rangle + |111\rangle + |001\rangle}{2} = |\psi_M\rangle. \end{aligned} \quad (\text{A.5})$$

However, $|\psi_M\rangle$ is not an eigenstate of the second Majorana tunneling term

$$\langle\psi_M|P_{14}|\psi_M\rangle = 0. \quad (\text{A.6})$$

The single-site reduced density matrices obtained from $|\psi_M\rangle$ are all maximally mixed. This leads to $S_1^M = S_2^M = S_3^M = S_{1\cup 2}^M = \log(2)$. The MI between the first and the second site is thus given by

$$I^M = S_1^M + S_2^M - S_{1\cup 2}^M = \log(2). \quad (\text{A.7})$$

To summarize, when two sites equally share a fermion, their MI reads $I^F = 2\log(2)$. By contrast, when they only share one Majorana, the MI is halved, i.e. $I^M = \log(2)$.

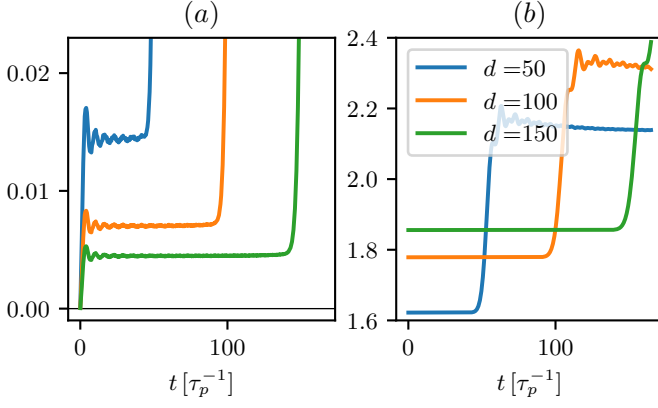


FIG. B1. Illustration of the initial offset of (a) the MI and (b) the EE of the probe for different sizes d of the spacing region X when coupled to the MZM. We show the amount of entanglement in units of $\log(2)$ with $N = 500, l = 4; (\mu^i = 20, \tau^i = \Delta^i = 1\tau_p) \rightarrow (\mu^f = 0, \tau^f = \Delta^f = 20\tau_p)$

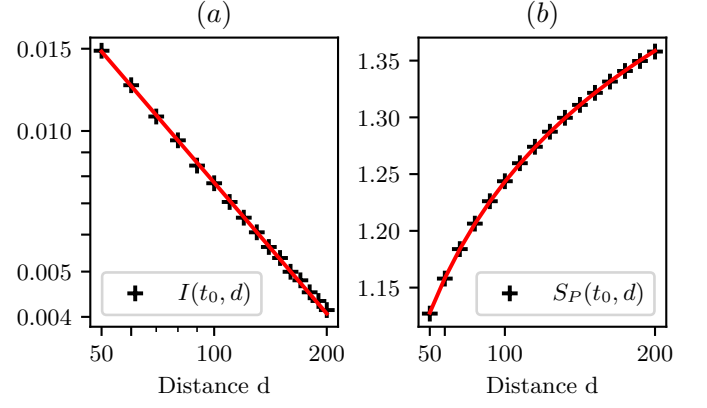


FIG. B2. Analysis of initial offset of (a) the mutual information $I(t_0, d)$ and (b) the EE $S_P(t_0, d)$ with respect to d , when coupled to the MZM. The MI is given in units of $\log(2)$, the EE in natural units. In (a) we numerically determine $I(t_0)$ as the value of $I(t)$ ($t \approx \delta t$) at the time $t_0(d)$ when the slope of the mutual information is above the threshold of $\frac{d}{dt}I(t) > 0.0005$. Due to the oscillations we smooth the data using a Savitzky-Golay filter before taking the numerical derivative. For (b) we choose $t_0 = 0$. As a guide to the eye a power law (red line) is fitted to the data, for the MI $I(t_0, d) \propto d^{-0.93}$. For the EE we use a logarithm to fit the data $S_P(t_0, d) \propto \log(d)/6.0 + \text{const.}$, which is the standard result known from literature [70]. Our parameter choice is (a) : $N = 1000$; (b) : $N = 2000, t_0 = 0; l = 4; (\mu^i = 20, \tau^i = \Delta^i = 1\tau_p) \rightarrow (\mu^f = 0, \tau^f = \Delta^f = 20\tau_p)$.

Appendix B: Initial entanglement value of EE and MI

In the main text (see Figs. 1,2 and 3), we focus on the entanglement entropy of the probe $\Delta S_P(t) = S_P(t) - S_P(0)$ and the mutual information $\Delta I(t) = I(t) - I(t_0)$ between the Q and P region, as only the change of those measures is important to observe the fractional entanglement value of the MZM. The aim of this section is to discuss more thoroughly the genuine measures $S_P(t)$ and $I(t)$ since both exhibit a finite value for times $0 \leq t < \delta t$ before the delay time δt . However, the origin of this initial value is completely different between the EE and MI, so we discuss them separately in the following.

B1. Initial entanglement entropy

In Fig. B1(b) we study $S_P(t)$ of the probe, when coupled to the MZM, from $t = 0$ to approximately $t \sim \delta t$ for several setups with varying distances d . Here, the important observation is that the $S_P(t)$ has a constant finite value from $t = 0$ until $t \sim \delta t$ and which is sizable with respect to the height of the (fractionalized) jump of $\log(2)/2$. The finite constant EE is due to the fact that we use a gapless probe when we couple to the MZM. It is well known that a subset (here the P -region) of a gapless system (here the XP -region) has a non-zero EE [69]. The initial value vanishes as soon as the probe becomes gapped for example when we couple to the fermionic bulk states.

It is expected that, for a gapless probe, the initial EE grows logarithmically with the size d of the X -region. We verify this in Fig. B2(b), where we plot $S_P(t_0, d)$ for several distances d and fit a logarithmic function (red curve) to the data points. It follows $S_P(t_0, d) \propto \log(d)/6 + \text{const.}$, in agreement with the result we expect for a 1D fermionic system with a single entanglement cut and a central charge $c = 1$ [66, 69–71].

B2. Initial mutual information

The MI behaves completely different to the EE for times $0 \leq t < \delta t$, as can be seen in Fig. B1(a), where we plot the MI when coupled to the MZM for several distances d . Initially, at $t = 0$, the MI is $I(t) \sim 0$ because the Q and P region are initially decoupled from each other. Then, we observe a time evolution consisting of damped oscillations, which eventually decay into a plateau at a small but finite value of I , see Fig. B1(a). The height of the plateau $I(t_0)$ is typically much smaller (two orders of magnitude in Fig. B1(a)) than the height of the jump occurring at $t \sim \delta t$. In addition, the height of the plateau $I(t_0)$ goes to zero as d increases (see Fig. B1(a) and Fig. B2(a)). It follows a powerlaw decay (red line in Fig. B2(a)). A non-vanishing (and time-dependent) MI before δt might seem puzzling, given the fact that the information about the quench reaches region P only after a time δt , as shown by the EE. However, the reason is that the MI is not a local quantity but, by definition, it involves the EE of Q , P and X . Right after the quench, region Q starts to be coupled only to the first sites of region X . They, however, are already weakly correlated with region P , given the gapless nature of H^{XP} . Those initial correlations are indeed expected to decay as a powerlaw with d (i.e. the distance of the sites from the entanglement cut between region X and P). This explains the non zero value of $I(t)$ below the Lieb-Robinson line for small d , which are visible Fig. 4 of the main text. We emphasize that $I(t_0)$ is very small for most values of d , so that it is fair to consider $\Delta I(t) \sim I(t)$ in most scenarios.

Appendix C: Quasiparticle dispersion in X region

We now focus on the long-time behavior of the MI, detailing how the limit value $\log(2)$ is reached when we couple to the MZM. For this reason, we define $f(t) = 1 - \Delta I(t)/\log(2)$, which measures the distance of the mutual information to 1 in units of $\log(2)$. In Fig. C1, we plot $f(t)$ on a double logarithmic scale for several setups. In Fig. C1(a), we vary the distance d , while in Fig. C1(b), we change the chemical potential μ_p in the XP region. Both have in common that during the delay time $t \leq \delta t$, when none of the entanglement particles emitted from Q have reached the probe region P , $f(t) = 1$ remains constant. However, after some transient for $t > \delta t$ we observe a power law decay of $f(t)$ towards zero.

In the following, we study how α depends on the system parameters. In particular, we show that it is independent of d (Fig. C1(a)) but, in general, it depends on the other parameters e.g. μ_p (see Fig. C1(b)). Neglecting some transient effects, we can give a rough description of the MI as:

$$I(t, d) = \begin{cases} 0 & t \leq \delta t(d) \\ \log(2) \left[1 - \left(\frac{t}{\delta t(d)} \right)^{-\alpha} \right] & t > \delta t(d) \end{cases} \quad (\text{C.1})$$

Here, $\delta t(d)$ and α depend on the system parameters we choose for a specific setup. The parameter α plays a particular role in the entanglement dynamics of our system as it determines the amount of correlation carried by modes of a specific velocity in the probe. In the following, we want to define more precisely the relation between α and the aforementioned velocity. Therefore, using Eq. (C.1), let us determine the time t_p needed to reach a certain level p of MI, say $I(t_p) = p \log(2)$ (with $0 < p < 1$). Then it follows that

$$\begin{aligned} p &= 1 - \left(\frac{t_p}{\delta t} \right)^{-\alpha} \\ \Rightarrow 1 - p &= \left(\frac{\delta t}{t_p} \right)^{\alpha} \\ \Rightarrow t_p &= \delta t (1 - p)^{-\frac{1}{\alpha}} \end{aligned}$$

with $\delta t = d/v_{\max}$. Hence, there is a linear relation between $t_p \propto d$, which we have already seen in Fig. 4 of the main text. There, the red dotted line corresponds to the contour of $I(t_p) = p \log(2)$ with $p = 0.95$.

From t_p , we can derive a velocity

$$v_p = \frac{d}{t_p} = v_{\max} (1 - p)^{\frac{1}{\alpha}}. \quad (\text{C.2})$$

We can thus interpret Eq. (C.2) as the velocity of the modes whose arrival in the probe region is associated with I reaching $I = p \log(2)$. This picture is consistent with the idea that several quasiparticles are emitted and travel

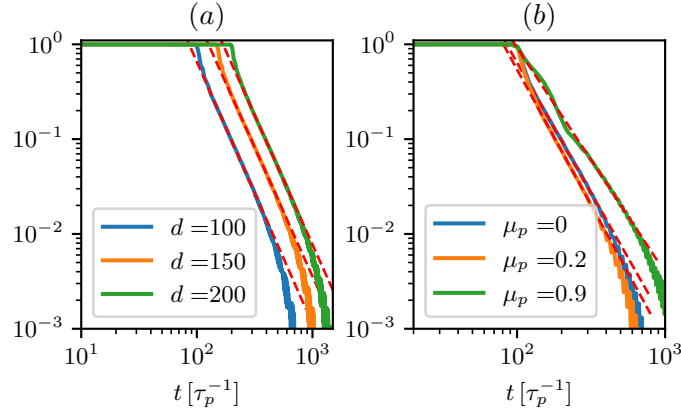


FIG. C1. Illustrations of how varying (a) the distance d and (b) the chemical potential μ_p affects the dispersion of the entanglement quasiparticles. For better visualization of the dispersion we plot the quantity $f(t)$ in units of $\log(2)$. There the red dashed lines show regions, where the decay follows a powerlaw. We choose (a) : $N = 1000$; (b) : $N = 800, d = 100, l = 4$; $(\mu^i = 20, \tau^i = \Delta^i = 1\tau_p) \rightarrow (\mu^f = 0, \tau^f = \Delta^f = 20\tau_p)$. For the plots (a), (b) we adapt the distance d respectively the potential μ_P (see legend entries).

independently in the probe, with different velocities according to their momentum and the dispersion relation of the probe, each one carrying a contribution to the MI. Large (small) values of α can be therefore associated with the fact that a large portion of the correlations is carried by fast (slow) modes.

That explains why varying d in Fig. C1(a) has no effect on the decay of $f(t)$, since the distribution of entanglement carried by modes with different velocity is independent of the distance d between the Q and the P region. A change of μ_p (see Fig. C1(b)) affects the aforementioned distribution of entanglement between the modes, leading to different decaying rates α of $f(t)$.

Appendix D: Robustness and sensitivity of the fractional entanglement signature

In the main text, we argue that the fractional entanglement signature is especially robust against deviations from the TSS and finite temperatures T , while being very sensitive to hybridization of the MZM. Hence, in the following we want to corroborate these statements.

D1. Sensitivity to hybridization

An important property of ΔI and ΔS_P is that they display a remarkable sensitivity to the presence of hybridization between the two MZMs hosted by the topological Kitaev chain (KC). To properly analyze this point, we consider an additional contribution to the Hamiltonian, which is already introduced in the main text:

$$H_{\gamma\gamma} = i\tau_{\gamma\gamma}\gamma_1\gamma_{2l} + \text{h.c.} \quad (\text{D.1})$$

It directly couples the Majorana operators γ_1 and γ_{2l} at the two ends of the KC and a finite amplitude $\tau_{\gamma\gamma} > 0$ leads to an hybridization of the two MZMs, which acquire a finite energy and, more importantly, cease to be isolated. The sensitivity of the entanglement signature to hybridization can be seen in Fig. D1(b), where we plot the values of $\Delta I(t)$ (orange line) and $\Delta S_P(t)$ (blue line) a long time $t = 3 \cdot 10^3 \tau_p^{-1}$ after the quench as a function of $0 \leq \tau_{\gamma\gamma} \leq 10^{-2} \tau_p$. Deviations from the quantized values can be observed already for $\tau_{\gamma\gamma} \sim 10^{-3} \tau_p$. This remarkable sensitivity to Majorana hybridization strongly points at the isolated nature of the right MZM as the origin of the anomalous quantized jumps observed in both ΔS_P and ΔI .

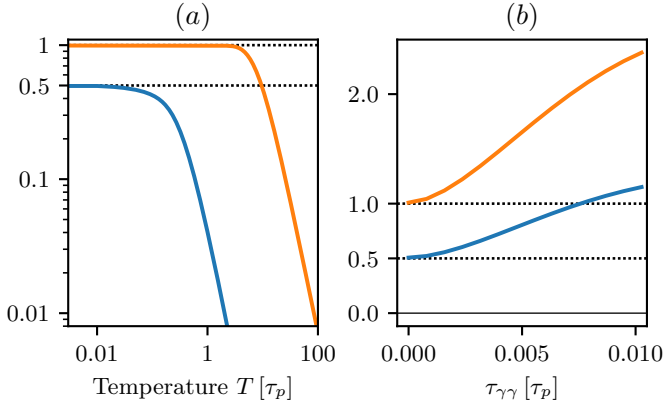


FIG. D1. ΔI (orange lines) and ΔS_P (blue lines), both in units of $\log(2)$, as a function of temperature T (panel (a)) and Majorana hybridization $\tau_{\gamma\gamma}$ (panel b) in the long time limit t_∞ . We choose $l = 4, d = 100, \tau_p = 1; (\mu^i = 20, \tau^i = \Delta^i = 1\tau_p) \rightarrow (\mu^f = 0, \tau^f = \Delta^f = 20\tau_p)$ and (a) : $N = 500, t_\infty = 500$; (b) : $N = 2000, t_\infty = 3000$.

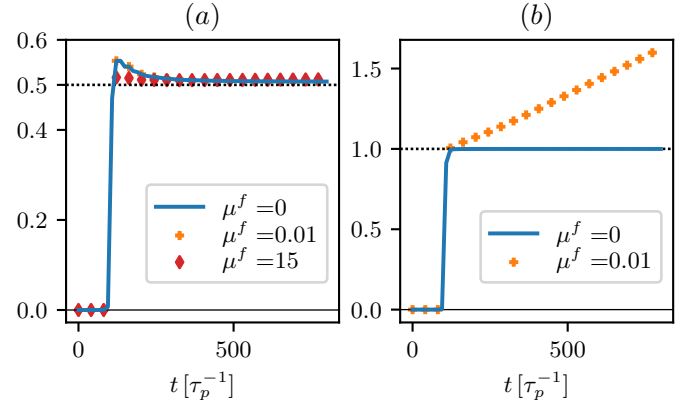


FIG. D2. Effects on the time dependence of ΔS_P when the quench deviates from the TSS. The parameter μ^f (in units of τ_p) is varied (see legend entries) and the time dependence of ΔS_P in units of $\log(2)$ is studied when coupled to (a) the MZM respectively (b) to the bulk states. Our choice of parameters is $N = 1000, d = 100, l = 34; (\mu^i = 20, \tau^i = \Delta^i = 1\tau_p) \rightarrow (\mu^f, \tau^f = \Delta^f = 20\tau_p)$.

D2. Robustness at finite temperature

In sharp contrast to the high sensitivity with respect to Majorana hybridization, the anomalous quantization of $\Delta I = \log(2)$ is particularly robust with respect to other parameters. In Fig. D1(a), we study the effects of finite temperature T . This amounts to consider the system to be initialized not in the groundstate $|\psi_0\rangle$ of H^i , but rather in the thermal state $\rho_{th}(T) = \sum_m \exp(-\varepsilon_m/T) |\psi_m\rangle \langle \psi_m|$, where $|\psi_m\rangle, \varepsilon_m$ are eigenstates respectively eigenenergies of H^i and $k_B = 1$. After a quench to the TSS, the quantization of $\Delta I = \log(2)$ (orange line) is perfectly retained up to temperatures slightly higher than the probe bandwidth, $T \gtrsim \tau_p$, but smaller than the topological gap, $T \ll \tau^f = \Delta^f$. This remarkable robustness at finite temperature strongly supports the topological origin of our phenomenon. The EE is more sensitive to the presence of thermal correlations. It displays a quantized jump in ΔS_P (blue line) only for $T \ll \tau_p$.

D3. Robustness against deviations from the TSS

Importantly, the anomalous quantization of ΔI and ΔS_P is retained also when the final Hamiltonian H^f is tuned away from the TSS (but still within the topological phase). In Fig. D2(a), it is clearly visible, that for a sufficiently long Q region ΔS_P converges to the fractional value of $\log(2)/2$ even for substantial deviations from the TSS (such as $\mu^f = 15\tau_p$, which is sizable with respect to $\tau^f = \Delta^f = 20\tau_p$). The same behavior can be observed in the MI. This robustness of the signature is not surprising since, as discussed in the main text, deviations from the TSS lead to two main effects: (i) an exponentially suppressed leaking of the edge MZMs towards the bulk of the KC and (ii) the presence of a finite bandwidth of the bulk states which implies a reduction of the topological gap E_{TG} .

Let us analyze those points in detail. Regarding point (i), in Fig. D3, it is shown how the hybridization of the MZMs affects the course of the ΔS_P and the fractional entanglement signature. There, for $\mu_f = 15\tau_p$, the hybridization is very small, leading to an energy splitting between the MZM of $\Delta E \sim 10^{-3}\tau_p$. As a result, according to Sec. D1, we expect the quantization to be retained until times of the order $t \sim 1000\tau_p$. As μ_p increases, the hybridization becomes more sizable. For $\mu_p = 15.5$ (orange dots), the splitting is $\Delta E \sim 3 \cdot 10^{-3}\tau_p$ and, indeed, we start to see a deviation from the blue line around $t \sim 300\tau_p^{-1}$. For $\mu_p = 16.5$ (green), the splitting is even larger ($\Delta E \sim 0.018\tau_p$) and $\Delta S_P(t)$ displays no fractional plateau. As for point (ii), using the expression for the bulk band dispersion, we see that even for the case of $\mu_f = 15\tau_p$ (as shown in Fig. D2(a) and Fig. D3) the topological gap $E_{TG} \sim 5\tau_p$ is still large enough so that the probe (with $\mu_p = 0$) is exclusively coupled to the MZM. Summarizing, as long as the topological gap remains large enough so that the probe can be exclusively coupled to zero energy modes (i.e. $|\mu_p| < \tau_p \ll E_{TG}$) and provided that the length l of the KC is long enough to prevent a detrimental hybridization between the exponentially localized MZM, effects (i) and (ii) are thus not expected to hinder the anomalous quantization of EE and MI.

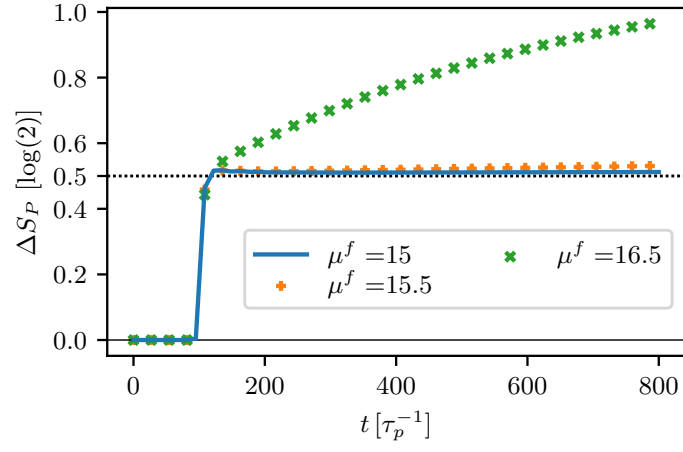


FIG. D3. Effects of hybridization of the MZMs on the time dependence of ΔS_P . The values of μ_f (in units of τ_p) are chosen in such a way that at $\mu_f = 15\tau_p$ the hybridization of the Majoranas is $\Delta E \sim 0.001\tau_p$, while for $\mu_f = 16.5\tau_p$ $\Delta E \sim 0.018\tau_p$. We choose $N = 800, d = 100, l = 34$; $(\mu^i = 20, \tau^i = \Delta^i = 1\tau_p) \rightarrow (\mu^f = 0, \tau^f = \Delta^f = 20\tau_p)$.

The situation is completely different when the probe is selectively coupled to the bulk of the KC. Indeed, while effect (i) has no consequences, the finite group velocity of the bulk band allows a large number of quench-generated quasiparticles above the topological gap to move from Q to X and eventually reach P . As a result, in the long time limit, ΔI and ΔS_P do not saturate anymore but rather tend to increase linearly (before finite size effects associated with finite l and N matter), as can be seen from Fig. D2(b).